Dual Specificity PDZ- and 14-3-3-Binding Motifs: A Structural and Interactomics Study

Gergo Gogl, Pau Jane, Célia Caillet-Saguy, Camille Kostmann, Goran Bich, Alexandra Cousido-Siah, Laszlo Nyitray, Renaud Vincentelli, Nicolas Wolff, Yves Nominé, et al.

Article

Structure

Dual Specificity PDZ- and 14-3-3-Binding Motifs: A Structural and Interactomics Study

Graphical Abstract

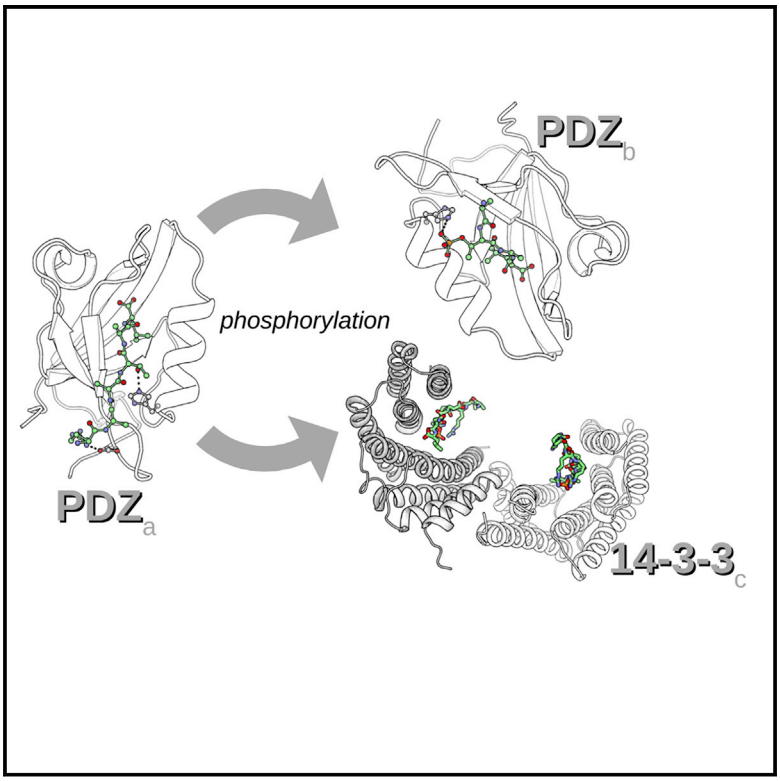

Authors

Gergo Gogl, Pau Jane, Célia Caillet-Saguy, ..., Yves Nomine, Nikolai N. Sluchanko, Gilles Trave

Correspondence

goglg@igbmc.fr (G.G.), nikolai.sluchanko@mail.ru (N.N.S.), traveg@igbmc.fr (G.T.)

In Brief

Gogl et al. studied the effects of phosphorylation of PDZ domain-binding motifs. They demonstrated that there are many phosphorylatable and phosphorylated motifs, some of which are also putative binding targets of 14-3-3 proteins. Using quantitative interactomic assays and crystallography they showed how phosphorylation and phosphomimetic substitution alters their binding properties.

Highlights

- A large proportion of PDZ-binding motifs are phosphorylatable
- Phosphorylated and phosphomimetic PBMs bind differently to PDZs and 14-3-3 proteins
- These differences are demonstrated by X-ray analysis and affinity profiling

Gogl et al., 2020, Structure *28*, 1–13
June 2, 2020
https://doi.org/10.1016/j.str.2020.03.010

CellPress

Please cite this article in press as: Gogl et al., Dual Specificity PDZ- and 14-3-3-Binding Motifs: A Structural and Interactomics Study, Structure (2020), https://doi.org/10.1016/j.str.2020.03.010

Structure
Article

Dual Specificity PDZ- and 14-3-3-Binding Motifs: A Structural and Interactomics Study

Gergo Gogl,[1,6,7,*] Pau Jane,[1,6] Célia Caillet-Saguy,[2] Camille Kostmann,[1] Goran Bich,[1] Alexandra Cousido-Siah,[1] Laszlo Nyitray,[3] Renaud Vincentelli,[4] Nicolas Wolff,[2] Yves Nomine,[1] Nikolai N. Sluchanko,[5,*] and Gilles Trave[1,*]

[1]Equipe Labellisee Ligue 2015, Department of Integrated Structural Biology, Institut de Genetique et de Biologie Moleculaire et Cellulaire (IGBMC), INSERM U1258/CNRS UMR 7104/Universite de Strasbourg, 1 rue Laurent Fries, BP 10142, 67404 Illkirch, France
[2]Récepteurs-Canaux, Institut Pasteur, UMR 3571, CNRS, 75724 Paris, France
[3]Department of Biochemistry, ELTE Eotvos Lorand University, Budapest, Hungary
[4]Architecture et Fonction des Macromolécules Biologiques (AFMB), CNRS UMR 7257, Aix-Marseille Université, Marseille, France
[5]A.N. Bach Institute of Biochemistry, Federal Research Center of Biotechnology of the Russian Academy of Sciences, 119071 Moscow, Russia
[6]These authors contributed equally
[7]Lead Contact
*Correspondence: goglg@igbmc.fr (G.G.), nikolai.sluchanko@mail.ru (N.N.S.), traveg@igbmc.fr (G.T.)
https://doi.org/10.1016/j.str.2020.03.010

SUMMARY

Protein-protein interaction motifs are often alterable by post-translational modifications. For example, 19% of predicted human PDZ domain-binding motifs (PBMs) have been experimentally proven to be phosphorylated, and up to 82% are theoretically phosphorylatable. Phosphorylation of PBMs may drastically rewire their interactomes, by altering their affinities for PDZ domains and 14-3-3 proteins. The effect of phosphorylation is often analyzed by performing "phosphomimetic" mutations. Here, we focused on the PBMs of HPV16-E6 viral oncoprotein and human RSK1 kinase. We measured the binding affinities of native, phosphorylated, and phosphomimetic variants of both PBMs toward the 266 human PDZ domains. We co-crystallized all the motif variants with a selected PDZ domain to characterize the structural consequence of the different modifications. Finally, we elucidated the structural basis of PBM capture by 14-3-3 proteins. This study provides novel atomic and interactomic insights into phosphorylatable dual specificity motifs and the differential effects of phosphorylation and phosphomimetic approaches.

INTRODUCTION

Short linear motifs are peptide segments that are disordered in isolation yet fold upon complex formation with globular domains, thereby participating in protein-protein interaction (PPI) networks (Davey et al., 2012). Consensus sequence features help to define families of motifs, which generally correspond to families of domains that recognize these particular motifs (Kumar et al., 2019). Most domain-motif PPI networks are rather promiscuous, i.e., each individual domain can interact with numerous distinct motifs, and vice versa (Ivarsson and Jemth, 2019). Furthermore, domain-motif networks are often modulated by post-translational modifications (PTMs). The most abundant PTM is phosphorylation, a reversible biochemical reaction, catalyzed by protein kinases and reverse catalyzed by protein phosphatases, that transfers the γ-phosphoryl group of an ATP molecule to a receiver residue, most often to the hydroxyl group of a Ser/Thr, or Tyr residue via forming a phosphoester bond (Hunter, 2012). Phosphorylated amino acids have unique properties that can alter biochemical properties of substrate proteins in different ways. Many *in vitro* and *in cellulo* experiments involve "phosphomimetic" acidic (Glu/Asp) mutations that are easy to introduce by recombinant approaches and are meant to reproduce the biochemical effect of site-specific phosphorylation events, despite being chemically distinct (Sieracki and Komarova, 2013). Across evolution of orthologous proteins, acidic amino acids are often seen to replace phosphorylated sites, and conversely (Pearlman et al., 2011).

PDZs are globular protein domains displaying a conserved antiparallel β barrel fold composed of five to six β strands and one to two α helices. PDZ domains recognize short conserved PDZ-binding motifs (PBMs) mostly located at the extreme C-terminus of their target proteins (Songyang et al., 1997). The sequences of C-terminal PBMs fall into three main classes (Luck et al., 2012). The last C-terminal residue (position 0) is almost always hydrophobic (mainly, Leu/Val/Ile). The third last residue (position -2) can be Ser/Thr (class 1), Val/Tyr/Phe (class 2), or Asp/Glu (class 3). The human proteome contains ~266 PDZ domains (the PDZome) dispersed over ~150 proteins, and a few thousand putative PBMs (Luck et al., 2012). This creates an extensive PDZ/PBM interactome, which is often hijacked by viral intruder proteins bearing their own PBMs (Javier and Rice, 2011; Banks et al., 2012; James and Roberts, 2016). Many PBMs are potentially phosphorylatable (Sundell et al., 2018). The phosphorylation of a PBM may cause a general change in its "PDZome-binding profile," namely the list of binding strengths exhibited by the PBM toward each individual human PDZ domain. This was recently demonstrated for ribosomal protein S6 kinase 1 (RSK1), a kinase from the Ras/ERK-MAPK pathway

Table 1. Ser/Thr Phosphorylatable PBMs: Summary of Our Bioinformatic Analysis of Human PBMs

	Class 1 PBM		Class 2 PBM		Class 3 PBM		All 3 Classes	
	Consensus	No. of Motifs	Consensus	No. of Motifs	Consensus	No. of Motifs	No. of Motifs	
	[ST]x[LVI]$	956	[VYF]x[LVI]$	458	[ED]x[LVI]$	512	1926	
	Phosphorylatable Class 1 PBM		Phosphorylatable Class 2 PBM		Phosphorylatable Class 3 PBM		All 3 Classes	
Position of Modification	Consensus	No. of Motifs	Consensus	No. of Motifs	Consensus	No. of Motifs	No. of Motifs	% of Total
-1	[ST]**[ST]**[LVI]$	172 (43)	[VYF]**[ST]**[LVI]$	73 (13)	[ED]**[ST]**[LVI]$	59 (15)	304	15.8
-2	**[ST]**x[LVI]$	956 (113)	not phosphorylatable by Ser/Thr kinases				956	49.6
-3	**[ST]**[ST]x[LVI]$	138 (12)	**[ST]**[VYF]x[LVI]$	80 (13)	**[ST]**[ED]x[LVI]$	63 (9)	281	14.6
-4	**[ST]**x[ST]x[LVI]$	134 (18)	**[ST]**x[VYF]x[LVI]$	56 (5)	**[ST]**x[ED]x[LVI]$	64 (13)	254	13.2
-5	**[ST]**x(2)[ST]x[LVI]$	144 (26)	**[ST]**x(2)[VYF]x[LVI]$	59 (8)	**[ST]**x(2)[ED]x[LVI]$	57 (13)	260	13.5
-6	**[ST]**x(3)[ST]x[LVI]$	165 (29)	**[ST]**x(3)[VYF]x[LVI]$	65 (10)	**[ST]**x(3)[ED]x[LVI]$	67 (14)	297	15.4
-7	**[ST]**x(4)[ST]x[LVI]$	138 (24)	**[ST]**x(4)[VYF]x[LVI]$	57 (14)	**[ST]**x(4)[ED]x[LVI]$	70 (14)	265	13.8
-8	**[ST]**x(5)[ST]x[LVI]$	120 (24)	**[ST]**x(5)[VYF]x[LVI]$	65 (12)	**[ST]**x(5)[ED]x[LVI]$	76 (15)	261	13.6
-9	**[ST]**x(6)[ST]x[LVI]$	137 (33)	**[ST]**x(6)[VYF]x[LVI]$	37 (6)	**[ST]**x(6)[ED]x[LVI]$	56 (9)	230	11.9
-10	**[ST]**x(7)[ST]x[LVI]$	123 (26)	**[ST]**x(7)[VYF]x[LVI]$	50 (9)	**[ST]**x(7)[ED]x[LVI]$	71 (16)	244	12.7
No. of phosphorylatable motifs		956		291		331	1,578	81.9
No. of phosphorylated motifs		218		65		92	375	19.5
No. of phosphorylatable sites		2,227		542		583	3,352	
No. of phosphorylated sites		348		90		118	556	

Putative phosphorylatable PBMs were searched using SLiMSearch (Krystkowiak and Davey, 2017), using a disorder score cutoff of 0.3. Note that we used the most restrictive definition of PBM consensus motifs according to the ELM database (Kumar et al., 2019) and only focused on C-terminal PBMs. Numbers in parentheses indicate the number of motifs that were found to be phosphorylated in low- or high-throughput mass spectrometry datasets in the PhosphoSite database (Hornbeck et al., 2015). Phosphorylatable motifs contain at least a single Ser/Thr residue at their last 11 C-terminal sequences. Phosphorylated motifs are those found at least once in the PhosphoSite database on at least one site. Phosphorylatable Ser/Thr residues within consensus motifs are highlighted in bold. $ denotes the C terminus (-COOH). For further details, see Table S1.

which is regulated by auto-phosphorylation of its own C-terminal PBM (Gógl et al., 2019). In addition, phosphorylation of a PBM can also alter its interactions with other protein families. For example, the 14-3-3 family, which contains seven members in humans, can also recognize C-terminal motifs in a phosphorylation-dependent manner (Coblitz et al., 2006). Worthy of note, viral E6 oncoproteins of high-risk mucosal human papillomavirus (HPV) types responsible for cervical cancers (Suarez and Trave, 2018) comprise C-terminal PBMs, which are subjected to phosphorylation events prone to modulate their interaction with PDZ domains and 14-3-3 proteins (Boon and Banks, 2013).

PDZ/PBM interactions display weak affinities, with low-micromolar dissociation constants for the best binders (Luck et al., 2011). Thus, accurately measuring the steady-state dissociation constant of a PDZ/PBM interaction can be challenging. We developed a high-throughput experimental approach, called the holdup assay, that can accurately measure such weak interactions (with a limit of quantitation of up to 100–150 μM dissociation constant) (Vincentelli et al., 2015). We have specially adapted the holdup assay to the PDZ domain family, by cloning and expressing the 266 known human domains (Duhoo et al., 2019). The approach allows us to measure complete PDZome-binding affinity profiles of any peptide sequence with high sensitivity.

Here, we combined quantitative interactomics and crystallography to investigate the differential effects of phosphorylation and phosphomimetic substitution of two phosphorylatable PBMs found in the HPV16 E6 viral oncoprotein and the human RSK1 kinase. To this aim, we measured all the affinities of wild-type, phosphorylated, and phosphomimetic versions of RSK1 and E6 PBMs toward the 266 human PDZ domains. We crystallized wild-type and modified RSK1 and E6 PBMs with the second PDZ domain of MAGI1 (MAGI1_2). Finally, we solved the crystal structure of phosphorylated E6 PBM bound to 14-3-3σ.

RESULTS

Proteome-wide Identification of Ser/Thr Phosphorylatable PBMs

To evaluate the extent of human PBMs potentially modulatable by phosphorylation, we searched the human proteome with the "SLiMSearch" program (Krystkowiak and Davey, 2017) using the most restrictive definition of a PBM, defined by the "ELM" linear motif database (Kumar et al., 2019). This way, we identified 1,926 human PBMs (956 class 1, 458 class 2, and 512 class 3). In Table 1, we counted for each PBM class the number of potentially phosphorylatable Ser/Thr sites at different positions of these PBMs, as well as the numbers of such sites that have experimentally been proven to be phosphorylated *in cellulo* according to the PhosphoSite database (Hornbeck et al., 2015). We found that up to 82% (1,578) of the 1,926 predicted human PBMs bear one or more

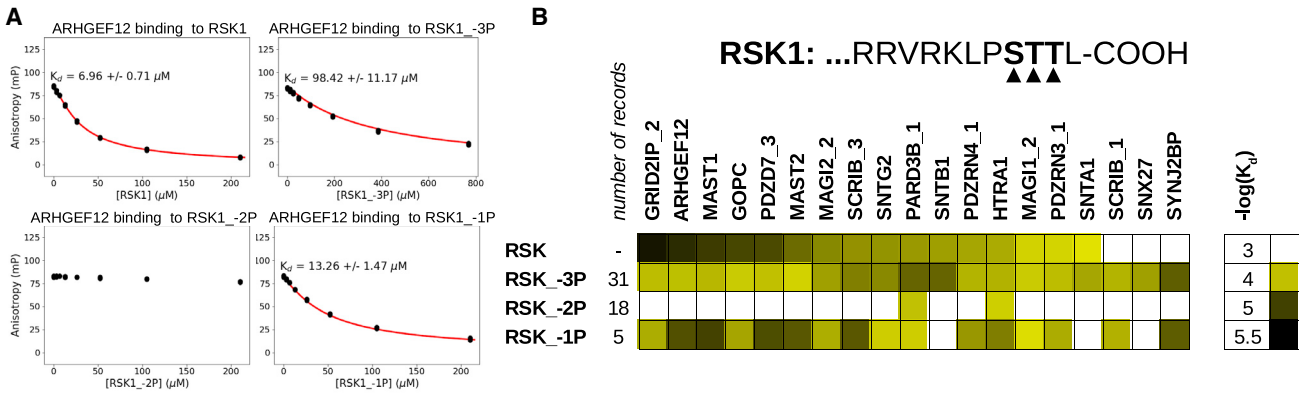

Figure 1. Affinity Measurements of Phosphorylated RSK1 Peptides with PDZ Domains

(A) Competitive fluorescence polarization assay was used to monitor 19 RSK interaction partners against four versions of the RSK1 PBM, native, or phosphorylated at position -1, -2, or -3. The interaction between the RSK1 and ARHGEF12 PDZ domains is shown as an example; all other data are shown in Figure S1.

(B) Heatmap of the measured interactions against the different, position-specific phospho-peptides. Based on the records of reported instances on the PhosphoSitePlus database, and also supported experimentally (Hornbeck et al., 2015; Gógl et al., 2018), RSK is most often modified at the -3 position and least often at the -1 position. Detectable interactions of RSK1 were modulated by phosphorylation at position -3 and -1 and were mostly eliminated by phosphorylation at position -2. The heatmap is colored by affinities, according to the scale bar on the right side.

potential phosphorylatable Ser/Thr sites between positions -1 and -10, and that 19% (375) have been found to be phosphorylated at least once on at least one site. In total, the predicted human PBMs contained, between positions -1 and -10, 3,352 potential and 556 experimentally proven potential phosphorylatable Ser/Thr sites (see also Table S1 for further details concerning a chosen subset of phosphorylatable class 1 motifs). Thus, phosphorylation of PBMs turns out to be very common, pointing to a dynamic regulation of their PPI interactome.

Class 1 PBMs, which systematically comprise a phosphorylatable Ser/Thr residue at position -2, are twice as frequent as class 2 or class 3 motifs and they harbor four times as many phosphorylatable sites. Worthy of note, phosphorylation of position -2 introduces an acidic charge, thereby creating a "pseudo-class 3 PBM," and its phosphomimetic substitution creates a class 3 PBM. The most common phosphorylated sites, proportionally to their occurrence, can be found at the position -1 of class 1 and class 2 PBMs. More than 25% of these sites (56 out of 245) are found to be phosphorylated *in cellulo*. In contrast, the least phosphorylated sites can be found at position -3 of class 1 PBMs. Less than 9% of these sites (12 out of 138) are found to be phosphorylated *in cellulo*. The most abundant PBM phosphorylation site affects position -2 of class 1 motifs with 113 experimentally proven instances.

The above list of phosphorylatable and/or phosphorylated PBMs is probably not exhaustive. As mentioned before, we used restrictive consensus motifs that may exclude several known PBMs (Vaccaro and Dente, 2002). For example, some functional PBMs may have a Cys, Met, and other residues at position 0 (Thomas et al., 2016), and others are not even positioned at the C terminus of proteins. Also, a number of phosphorylatable PBMs may only be modified under special conditions that have never been experimentally addressed. Finally, some phosphorylated PBMs may be difficult to detect by mass spectrometry (Lucrèce et al., 2011). For example, the HPV-E6 oncoproteins, whose expression is essential for HPV-transformed cells, such as HeLa, comprise a phosphorylatable PBM that is addressed in the present work. However, E6 oncoproteins are only expressed at a very low amount in cells and have a basic residue at position -4. Thus, a standard proteolytic digestion is expected to yield small amounts of a very small fragment, making it difficult to identify by mass spectrometry. Furthermore, the sequence of E6, being a viral protein, is not always present in standard lists of human proteins, so that a database search on the human proteome might skip E6-derived fragments.

Phosphorylation at Distinct Sites of the RSK1 PBM Differentially Impacts Its Binding Affinity for a Panel of PDZ Domains

The RSK1 kinase harbors a C-terminal class 1 PBM (…RRVRKLPSTTL-COOH) (Thomas et al., 2005). RSK1 can autophosphorylate its C-terminal tail at positions -3, -2, and -1, leading to a rearrangement in its PDZ specificity (Gógl et al., 2018). In addition, in the PhosphoSite database RSK1 PBM is the class 1 PBM most frequently phosphorylated at the -3 position (Table S1). Here, we used RSK1 to assess the potential impact of phosphorylation of different positions of a class 1 PBM on its binding affinity for PDZ domains. Based on previous results (Gógl et al., 2019), we selected 19 PDZ domains and tested their interactions with competitive fluorescence polarization assay against all possible (mono) phosphorylated RSK1 peptides (Figures 1 and S1). Within the detection range of fluorescence polarization, phosphorylation at position -2 apparently abolished most interactions, whereas phosphorylation at positions -3 and -1 rather modulated their binding affinities. Therefore, in terms of phosphorylation, the -2 position has a higher impact on PDZ interactions than the -3 and -1 positions. This corroborates a previous study that analyzed the effect of phosphorylation on the binding properties of 100 putative phosphorylatable PBMs, assayed against three distinct PDZ domains (Boisguerin et al., 2007).

PDZome-Binding Profiles of Native, Phosphorylated, and Phosphomimetic PBMs

For further studies, we set out to investigate at proteome-wide level how phosphorylation and phosphomimetic mutations

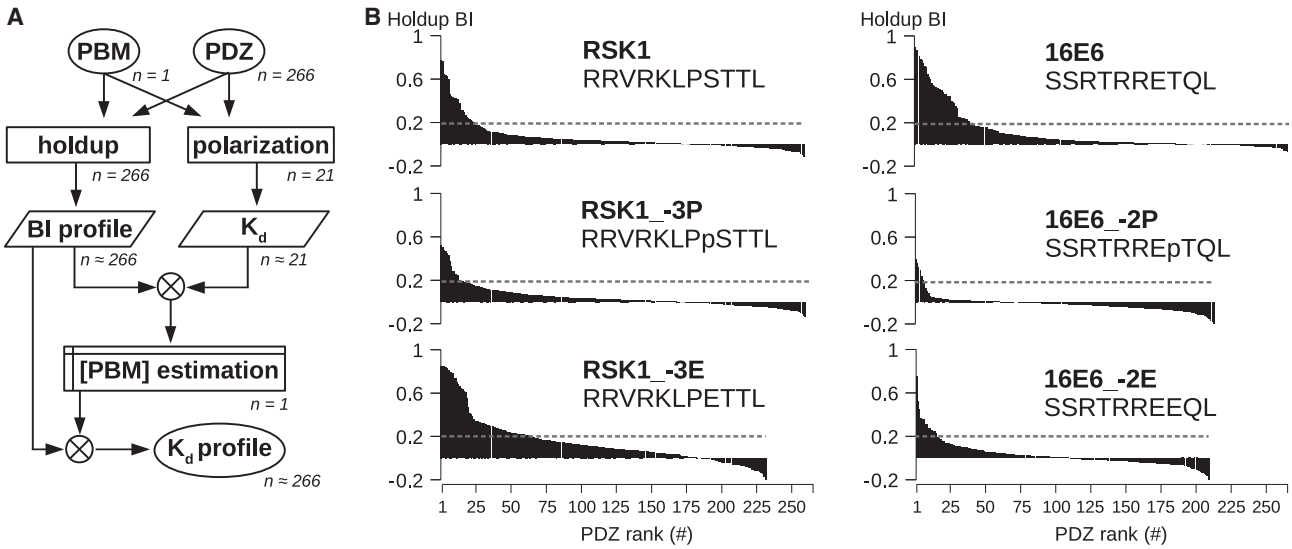

Figure 2. PDZome-Binding (BI) Profiles of the Studied PBMs, Measured by the Holdup Assay

(A) The general flowchart of the holdup assay and the conversion of binding intensities into dissociation constants with the aid of competitive fluorescence polarization assays. The holdup assay generates a BI profile that can be converted into steady-state dissociation constants, if we know the approximate peptide concentration during the holdup experiment. This concentration can be estimated using dissociation constants of a small set of interactions, determined by an orthogonal approach.

(B) BI profiles of the studied PBMs. Because each profile is ordered by decreasing BI values, the order of PDZ domains differs between panels. Gray dashed lines represent the conservative threshold of accurate binding quantitation by holdup assay (BI = 0.2).

directed at a higher- or a lower-impact position of class 1 PBMs would alter their full PDZome interactome. This question was addressed using the phosphorylatable PBMs of RSK1 kinase and of HPV16 E6 oncoprotein (herein defined as 16E6). The PBM of 16E6 (… SSRTRRETQL-COOH) harbors phosphorylatable sites at positions -2, -6, -8, and -9, and it was proven to be phosphorylated by various kinases at position -2 (e.g., by basophilic kinases due to a basic patch at position -5, such as PKA) (Kühne et al., 2000). To generate PDZome-binding profiles of RSK1 and 16E6 PBM variants, we performed holdup assays (Vincentelli et al., 2015) using an updated version of our PDZ library, which includes individual clones of all possible 266 PDZ domains as MBP-fused proteins (Duhoo et al., 2019). We measured the binding profiles of the 16E6 peptides (native, SSRTRRETQL; phosphorylated, SSRTRREpTQL; phosphomimetic, SSRTRREEQL) against all human PDZ domains. In the case of RSK1, we had previously determined the binding profiles of the native (RRVRKLPSTTL) and the phosphorylated (RRVRKLPpSTTL) peptides (Gógl et al., 2019). Here, we measured the binding profile of the phosphomimetic peptide (RRVRKLPETTL) along with an additional reference profile of the phosphorylated peptide (Figures 2 and S2; Table S2).

In a holdup experiment, a cell lysate containing an overexpressed PDZ domain of known concentration is incubated with a peptide-saturated resin, the mixture is rapidly filtered, and the remaining PDZ concentration in the filtrate is measured. The experiment provides, for each PDZ domain, a steady-state depletion factor (binding intensity, or BI), that can in principle be converted into a steady-state dissociation constant. This conversion is necessary if we need to compare multiple binding profiles, as each peptide might reach a different concentration during resin saturation. Estimating the dissociation constant requires access to three concentrations: free PDZ, free peptide, and PDZ-peptide complex. As stated above, the holdup assay delivers, for each PDZ-PBM pair, the concentrations of free PDZ and complex, while the concentration of free peptide remains unknown. However, using an orthogonal approach, we can obtain steady-state dissociation constants for a subset of PDZ-PBM pairs. We can then use these dissociation constants to back-calculate the peptide concentration in the holdup assay, which is expected to be the same for all PDZ-PBM pairs in that assay. We used a competitive fluorescence polarization assay and measured the binding affinities of the 6 studied peptides against 21 purified PDZ domains (Figure S1) (Roehrl et al., 2004). In the holdup assay, we had already determined the corresponding BI values for most of these 126 interactions. We complemented the binding profiles with 9 interactions that we only measured with the fluorescence polarization assay in Table S2. For each given interaction, where both a quantifiable (>0.2) BI value and a dissociation constant were available, we calculated the apparent peptide concentration present in the holdup assay. Then, we used the average peptide concentrations obtained in that way to convert the original BI profiles into profiles displaying actual dissociation constants (Figure 3A). In the case of the modified 16E6 peptides, we only detected very weak interactions with the holdup assay that we failed to detect with fluorescence polarization. For these peptides, we used the average of the other peptide concentrations (of RSK1s and 16E6) for the conversion.

Holdup experiments for 16E6_-2P, 16E6_-2E, and RSK1_-3E were performed in singlicate. These singlicate holdup runs provided highly reliable data, as shown by the strong agreement of dissociation constants obtained from holdup assays and fluorescence polarization assays (Figure 3B). Based on our previous experience, the holdup assay is highly sensitive with a limit of

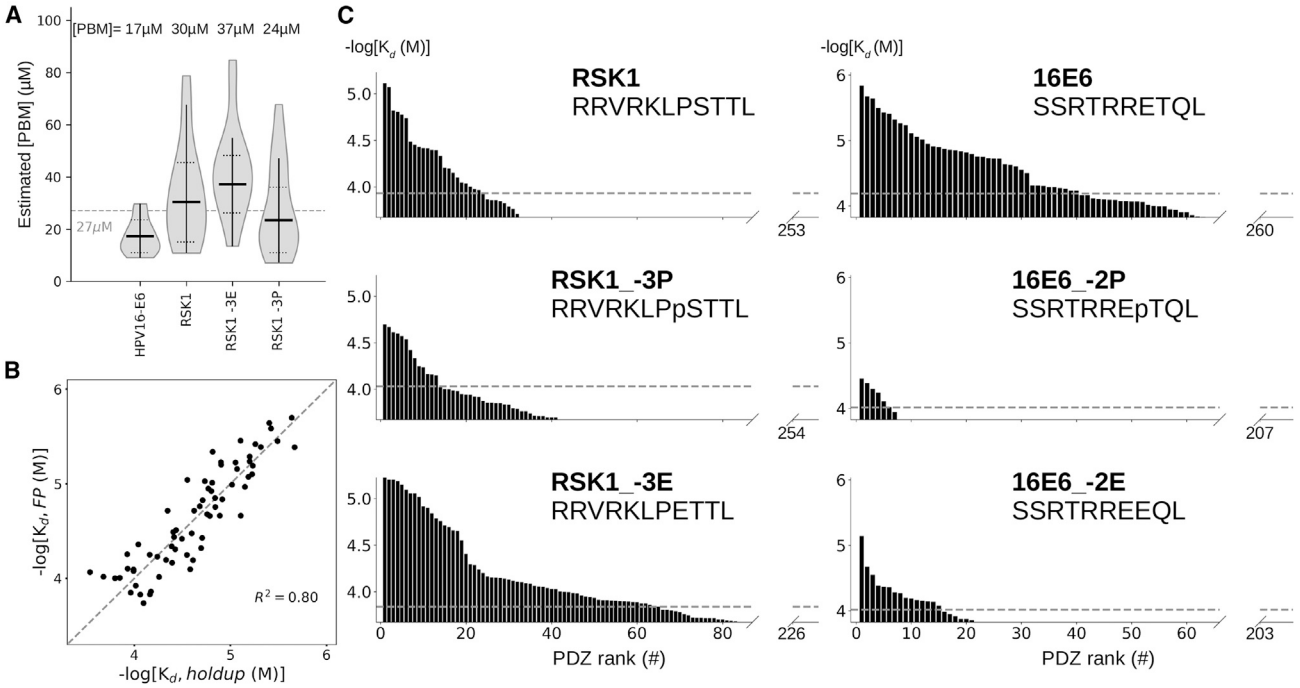

Figure 3. PDZome-Binding (K_d) Profiles of the Studied PBMs, Measured by the Holdup Assay

(A) Determined PBM peptide concentrations in the holdup assay, based on competitive fluorescence polarization experiments. Vertical lines in the violin plot show the minimal and maximal observed peptide concentration after outlier rejection. Horizontal lines show the mean and the standard deviation of the peptide concentration after outlier rejection. The gray dashed line shows the average peptide concentration that was used to convert the 16E6_-2P, 16E6_-2E profiles.

(B) Correlation of dissociation constants determined by the two orthogonal biochemical methods.

(C) K_d profiles of the studied PBMs. Because each profile is ordered by K_d values, the order of PBZ domains differs between panels. For clarity, we omitted most of the undetected binders. Gray lines represent the limit of accurate binding quantitation by the holdup assay (BI = 0.2).

detection of BI = 0.1 (10% PDZ depletion in solution) when experiments are run in triplicate (Vincentelli et al., 2015). Here, based on our comparison with fluorescence polarization, and on the fact that the holdup assays were run in singlicate, we set a conservative lower limit of quantitation at BI = 0.2 (20% PDZ depletion in solution), roughly corresponding to a 100 μM dissociation constant (Figure 3C).

Interactomic Consequence of Phosphorylation or Phosphomimetics of RSK1

Using the holdup assay, we were able to measure the interaction of RSK1 against 259, 260, and 232 PDZ domains for the native, phosphorylated, and phosphomimetic peptides, accounting for 97.4%, 97.7%, and 87.2% of coverage of the complete human PDZome, respectively (Figure 4). Using the threshold of BI = 0.2 for a quantifiable interaction, we detected 23, 13, and 67 significant interactions for the native, phosphorylated, and phosphomimetic peptides, respectively (8.9%, 5%, and 28.9% of the tested PDZome). Phosphorylation at position -3 generates a decrease in overall affinity and reorganizes the preferences of the RSK1 PBM for individual PDZ domains. Compared with the native RSK1 PBM, phosphorylated RSK1 retains, loses, and gains 10, 13, and 3 detectable partners, respectively. ARHGEF12 (an important substrate of RSK) (Shi et al., 2018) is among the lost binders, while SYNJ2BP is among the gained ones.

The phosphomimetic mutation also reshuffles the individual PDZ binding preferences of the native RSK1 PBM, but in contrast to phosphorylation it globally enhances the affinities in the binding profile, resulting in a larger number of detected interaction partners. Compared with the native RSK1 PBM, the phosphomimetic PBM retains, loses, and gains 22, 1, and 45 detectable partners, respectively. Overall these data point to strong differences between the phosphorylated and phosphomimetic RSK1 PBMs. Although phosphorylation strongly reorganizes the RSK1 PBM interactome, with numerous losses and gains of binders detected within a given affinity range, the phosphomimetic mutation expands the RSK1 interactome by increasing the number of detected binders without almost any loss. Far from accurately mimicking the phosphorylated state, the phosphomimetic peptide is essentially a very promiscuous peptide that binds all partners of both native and phosphorylated RSK1 PBM, plus numerous additional ones.

Structural Consequence of Phosphorylation or Phosphomimetics of RSK1

Previously, we determined crystal structures of the MAGI1_2 PDZ domain bound to the native RSK1 and RSK1_-3P peptides (Gógl et al., 2018). The PDZ domain was fused to Annexin A2 to enhance crystal formation, which enabled us to gain molecular insight into these PDZ/PBM complexes (Ecsédi et al., 2020). We used the same construct to obtain the complex with the

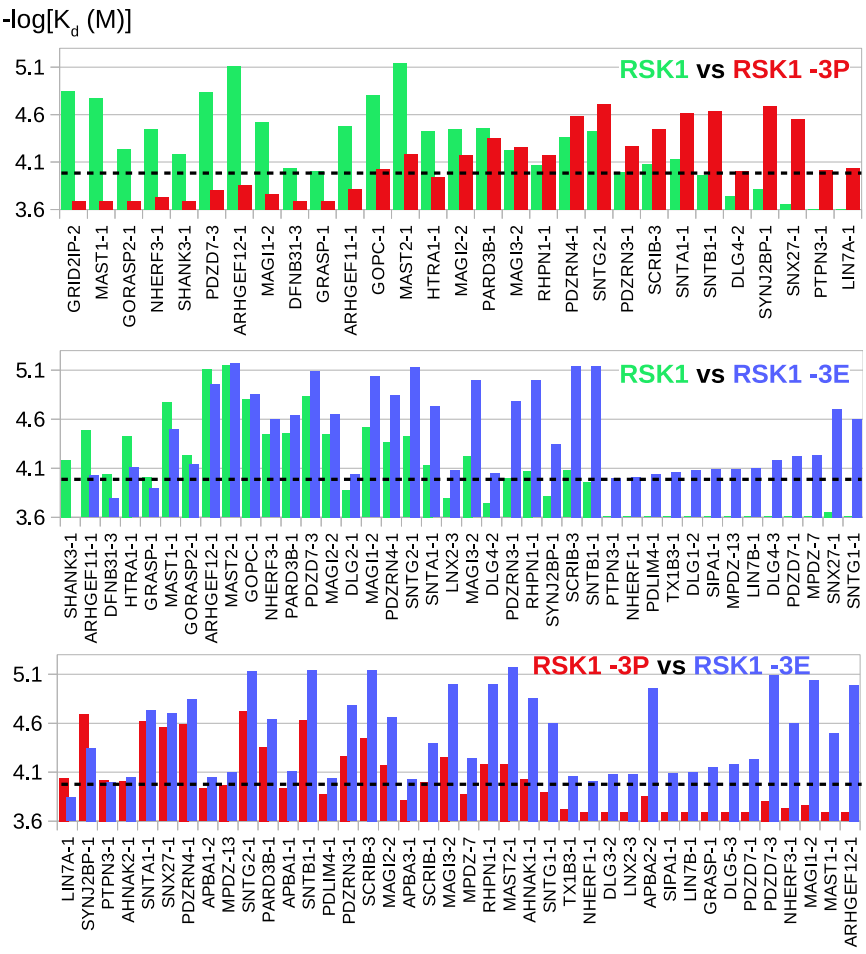

Figure 4. Pairwise Rearrangements in PDZome-Binding K_d Profiles of the Studied RSK1 PBMs

The PDZs are ordered by the determined fold-change (ΔΔG) between the two compared motifs. Dashed line represents the averaged limit of accurate binding quantitation by the holdup assay (BI = 0.2; [PBM] = 27 μM; K_d = 105 μM).

phosphomimetic RSK1 peptide (Figure 5; Table S3). In the crystal, MAGI1_2 exhibits the common PDZ fold consisting of five β strands and two α helices. The RSK1 peptides bind to the conventional binding groove of the PDZ domain (outlined by β-2, α-2, and the carboxylate-binding "GLGF loop").

The RSK1 peptides establish all canonical interactions of a class 1 PBM (Hung and Sheng, 2002). As a C-terminal anchor, the C terminus of the peptide interacts with the carboxylate-binding loop and the peptide adopts an antiparallel β strand conformation, which complements the exposed β-2 strand of the PDZ fold. A Thr residue at position -2 of the PBM mediates a hydrogen bond with His530 from the α-2 of the PDZ domain. Upon phosphorylation, this conformation is maintained, but some minor local conformation changes were observed around the phosphorylation site. Lys499 is located on the β-3 strand of the PDZ and its side chain is solvent-exposed, facing the -3 position of a PBM. As already observed in previous works (Zhang et al., 2007; Charbonnier et al., 2011), Lys499 is at an ideal position to mediate specific interactions with PBMs. Indeed, an interaction was observed between this residue and the Ser at position -3 of the RSK1 PBM (with a distance of 2.9 Å). Upon phosphorylation, this phospho-Ser residue was captured in two different rotamer conformations (in two closely related crystals), but both of them formed an interaction with the side chain of Lys499 (with a distance of 2.7–3.5 Å) (Gógl et al., 2018). The phosphomimetic peptide forms a similar interaction with the same amine group (with a distance of 2.2 Å).

Interactomic Consequence of Phosphorylation or Phosphomimetics of HPV16 E6

Using the holdup assay, we were able to measure the interaction of 16E6 PBM against 266 PDZ domains for the native peptide, 213 for the phospho-peptide, and 209 for the phosphomimetic peptide (Figure 6). These account to 100.0%, 80.1%, and 78.6% of coverage of the complete human PDZome, respectively. Using the limit of quantitation of our singlicate holdup assay (BI = 0.2, corresponding to a dissociation constant of 60–100 μM), we detected 41 significant interactions for the native-, 6 for the phospho-, and 15 for the phosphomimetic peptide (15.4%, 2.8%, and 7.2% of the tested PDZome, respectively). Moreover, the detected interactions of the modified peptides were markedly weaker compared with the average binding affinity of the native motif. In many cases, we failed to confirm the binding of these weak partners of the phosphorylated and the phosphomimetic peptides with the fluorescence polarization assay (Figures S1 and S3). Thus, we hardly detected any significant interaction partners upon modification of the HPV16-E6 motif at the -2 position.

Upon phosphorylation, 16E6 lost all of the experimentally significant binders of the native peptide with the exception of the weak binder FRMPD4 (Figure S3). Upon phosphomimetic substitution, 16E6 lost 31 significant binders of the native peptide. In addition, only a small overlap (consisting of 3 detected binders) was detected between the identified weak interaction partners of the phospho- and the phosphomimetic 16E6 PBM. An analogous phosphomimetic substitution on the 18E6 PBM was previously found to dramatically reduce its ability to interact with SNX27 (Ganti et al., 2016).

Structural Consequences of Phosphorylation or Phosphomimetics of HPV16 E6

MAGI1_2 is one of the strongest PDZ partners of 16E6 but, upon 16E6 phosphorylation at position -2, its affinity fell below the detection limits of both holdup and standard fluorescence polarization assays (Figure S1; Table S2). To estimate the very weak affinity of this complex, we repeated the competitive

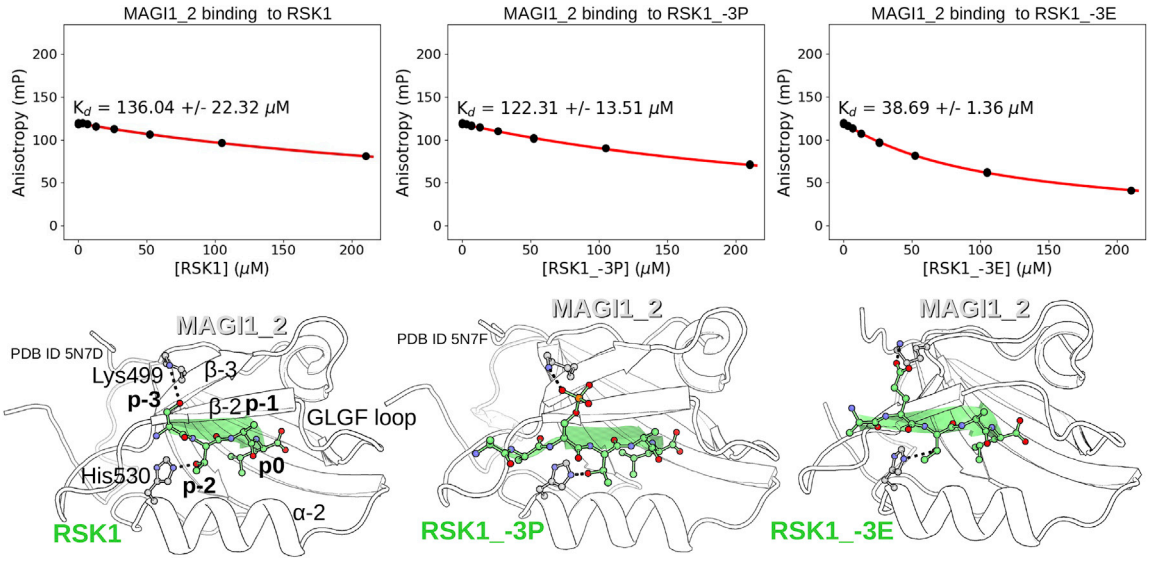

Figure 5. Crystal Structures Show the Molecular Consequence of RSK1 Phosphorylation on MAGI1_2 PDZ Binding

Isomorphous MAGI1_2-bound RSK1 peptides are shown in parallel with their affinities. Competitive fluorescence polarization assay was used to monitor the binding of RSK1 peptides to this PDZ domain (see Figure S2 for further details). RSK1 is modified at its position -3, facing Lys499 of MAGI1. The interaction between these residues remains possible, independently of the presence of the phosphorylation or the mutation. The crystal structures of MAGI1_2, bound to RSK1 (left panel) and RSK1_-3P (middle panel) were solved in our previous work (PDB: 5N7D and 5N7F) (Gógl et al., 2018). See Table S3 for statistical details about crystallographic data collection and refinement.

fluorescence polarization experiment by extending the range of titration from 200 μM to 2.5 mM. Under this modified condition, we managed to estimate the dissociation constants both for 16E6_-2P ($K_d \sim 2.5$ mM) and for 16E6_-2E ($K_d \sim 1$ mM) (Figure 7). Despite these fairly weak associations, we managed to crystallize both complexes, as well as a third complex, including wild-type 16E6 peptide, using the Annexin A2-fused MAGI1_2 construct. To push the reaction toward complex formation, we used an overall PDZ concentration of 135 μM (just as before), supplemented with 2 mM of modified peptides. In a crystal of this fused PDZ domain, the concentration of the PDZ site is approximately 11 mM (based on the typical unit cell dimensions and space group of the obtained crystals). In this situation, approximately 44% complex formation should be expected with the phosphorylated peptide. However, this calculation does not take into account synergistic effects within the crystal, which might significantly increase the fraction of complex formed. Indeed, co-crystallization resulted in isomorphous crystal with high peptide occupancy.

The 16E6 peptide adopts a classical PBM fold, satisfying all the required interactions with the PDZ domain of MAGI1 (Figure 7; Table S3). As described previously in detail (Charbonnier et al., 2011; Zhang et al., 2007), the 16E6 PBM mediates several bonds with the PDZ domain, including a side-chain-mediated contact between Glu494 of MAGI1 (of the β-2, β-3 loop) and an Arg from position -5 of the PBM. In contrast, in the phosphorylated complex the classical β strand structure of the PBM is disrupted. Here, the only interaction reminiscent of a class 1 motif is that involving the C terminus of the PBM and the GLGF loop of the PDZ. The Thr residue at position -2 is unable to mediate a bond with its hydroxy group with His530 from the α-2, because it is part of the phosphoester bond. This is somewhat compensated by a weak interaction between one of the oxygen atoms of the phosphate group and the imidazole ring of His530. The main chain of the PBM has moved away, impeding the β strand conformation of the bound peptide. The structure of the phosphomimetic peptide is similar, although not identical. We do not observe any direct contact between the acidic residue and His530, but the interactions of the peptide are similarly limited to the extreme C terminus. Thus, both the phosphorylation and the phosphomimetic mutation at position -2 resulted in a significant alteration in the bound β conformation of the PBM.

Phosphorylated PBMs Are Also Potential 14-3-3 Binding Motifs

C-Terminal motif binding is not an exclusive property of PDZ domains. For example, PBM phosphorylation can also create an alternative binding site for 14-3-3 proteins (Espejo et al., 2017). To test the possibility of these alternative interactions, we measured the interactions of 14-3-3σ with the PBM of RSK1, a kinase that was previously shown to interact with 14-3-3 proteins (Cavet et al., 2003). Although RSK1 did not detectably interact, RSK1_-3P showed indications of a weak phosphorylation-dependent interaction, and both RSK1_-2P and RSK1_-1P bound strongly to the tested 14-3-3σ (Figures 8A and S4). RSK1_-2P and RSK1_-1P are, according to experimental data, the minor PBM autophosphorylation sites of RSK1 (Figure 1) (Hornbeck et al., 2015; Gógl et al., 2018). All three phosphopeptides fit to the documented consensus of mode III 14-3-3-binding motifs (Figure 8B). 14-3-3 interactions are centered around the phosphate moiety, and mode III 14-3-3-binding motifs are C-terminal motifs phosphorylated at position -1, -2, or sometimes -3 relative to the C terminus, with Pro being excluded immediately after the phospho-residue (Kumar et al., 2019; Panni et al., 2011; Sluchanko, 2018). The latter

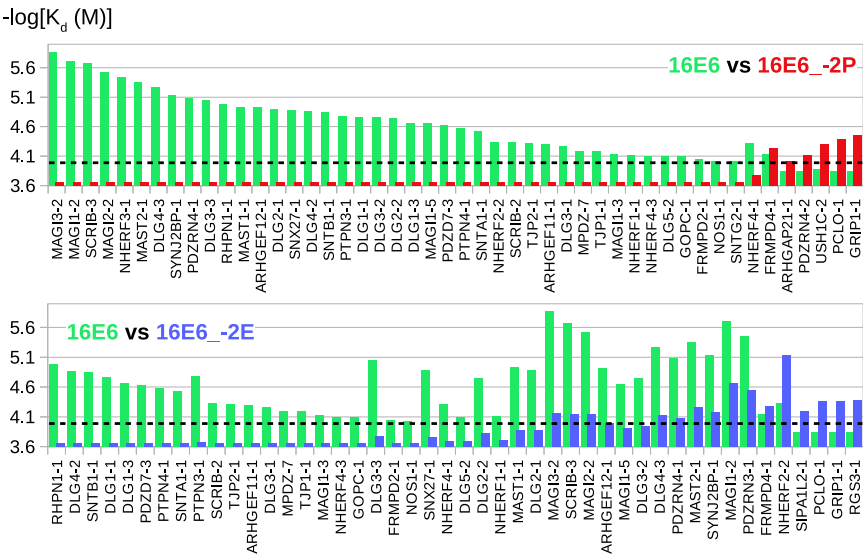

Figure 6. Pairwise Rearrangements in PDZome-Binding K_d Profiles of the Studied 16E6 PBMs

The PDZs are ordered by the determined K_d ratio ($\Delta\Delta G$) between the two compared motifs. Dashed line represents the average limit of accurate binding quantitation by the holdup assay (BI = 0.2; [PBM] = 27 μM; K_d = 105 μM).

restriction excluding proline only affects class 1 PBMs that are phosphorylated at position -2 (Figure 8B; Table S1). Among a large number of PBMs phosphorylatable at such positions, only 29 putative and 5 detectably phosphorylated PBMs do not satisfy the requirements of the mode III 14-3-3-binding consensus (34 in total out of all 956 class 1 motifs). Thus, all the remaining phosphorylatable PBMs (1,507 putative motifs) are also potential 14-3-3 binders (Figure 8C).

Crystal Structure of 14-3-3σ Protein Bound to Phosphorylated HPV16 E6 PBM

The HPV E6 oncoproteins were already described as interaction partners of several 14-3-3 proteins (Boon and Banks, 2013; Boon et al., 2015). We found that the C-terminal PBM of 16E6 can mediate phosphorylation-dependent interaction with 14-3-3σ, a well-characterized member of the 14-3-3 family (Figure 9A). We went on to solve their co-crystal structure using a crystallization-optimized protein (Sluchanko et al., 2017). As observed for most 14-3-3 binding motifs, the phosphate group is very well coordinated by the 14-3-3σ protein (Figure 9B) (Obsil and Obsilova, 2011; Sluchanko et al., 2017). It interacts with several residues of the 14-3-3 protein (e.g., Arg56, Arg129, and Tyr130) and it is also stabilized intra-molecularly by an Arg residue from position -4 of the same PBM peptide. In addition, the peptide forms several main-chain-mediated bonds, including an interaction between the C terminus of the PBM and Lys122 of 14-3-3σ. The Arg residue at position -5 of the PBM is involved in a stacking interaction with Arg60 of 14-3-3σ.

In contrast to the phosphorylated 16E6 PBM, the phosphomimetic 16E6 PBM did not detectably interact with 14-3-3σ (Figures 9A and S4), confirming previous data showing that a phosphomimetic 18E6 PBM failed to interact with 14-3-3ζ (Boon and Banks, 2013). In line with these observations, our phospho-PBM-bound 14-3-3 structure shows a strict coordination of the phosphate group. An acidic mutation would be inadequate to mediate the same mode of binding, as already observed for other binding partners of 14-3-3 proteins (Zheng et al., 2003).

DISCUSSION

New Perspectives in Quantitative Interactomics

In this work, we have quantitatively assessed a very large number of affinities, for ~1,500 distinct PDZ-peptide pairs. Although we obtained binding constants for ~170 pairs, we also showed that the remaining ~1,330 pairs displayed affinities below our quantitation threshold. Both types of data are important for building our understanding of interaction networks. Although the former inform us on the "interactome," the latter inform us on its complementary, often neglected side: the "negatome," comprising all non-favored interactions in the network.

The Consequences of PBM Phosphorylation

Although the human proteome contains thousands of putative phosphorylation sites within PBMs (Table 1), the only case when a PTM may target a high-impact, key motif position for PDZ binding are class 1 motifs phosphorylatable at position -2. All other modification sites affect lower-impact, modulatory positions.

Our results demonstrate that phosphorylation at position -3 of the RSK1 PBM reorganizes its PDZome-binding profile by increasing its affinity for some PDZ domains and decreasing it for others. This rearrangement in the RSK1 interactome can be measured both *in vitro* and *in cellulo* (Gógl et al., 2019). Phosphorylation at key position -2 of 16E6 outlines a more drastic effect as it suppresses most of the detectable interactions of the native motif, as shown by our structural data, by disrupting the β conformation of the bound peptide. This finding supports the previously described phospho-dependent disruption of different E6 PBMs with several PDZ domains and the phospho-regulation of other, non-viral PBMs (Boon et al., 2015; Cohen et al., 1996).

Although phosphorylation at a key motif position can disrupt molecular interactions to a degree that makes them undetectable with standard methods, phosphorylation at lower-impact sites tends to preserve the overall bound conformation, while modulating affinity and specificity profiles. As an example, the PBM of β2AR (… CSTNDSLL-COOH) harbors three phosphorylatable residues (Clairfeuille et al., 2016). Although the native β2AR PBM binds moderately to the PDZ domain of SNX27, its variants phosphorylated at modulatory positions -5 and -6 bind more strongly, and the variant phosphorylated at key position -2 binds significantly more weakly. Yet, solution NMR experiments showed that the chemical environment of the carboxylate-binding GLGF loop was altered in presence of the -2 phosphorylated

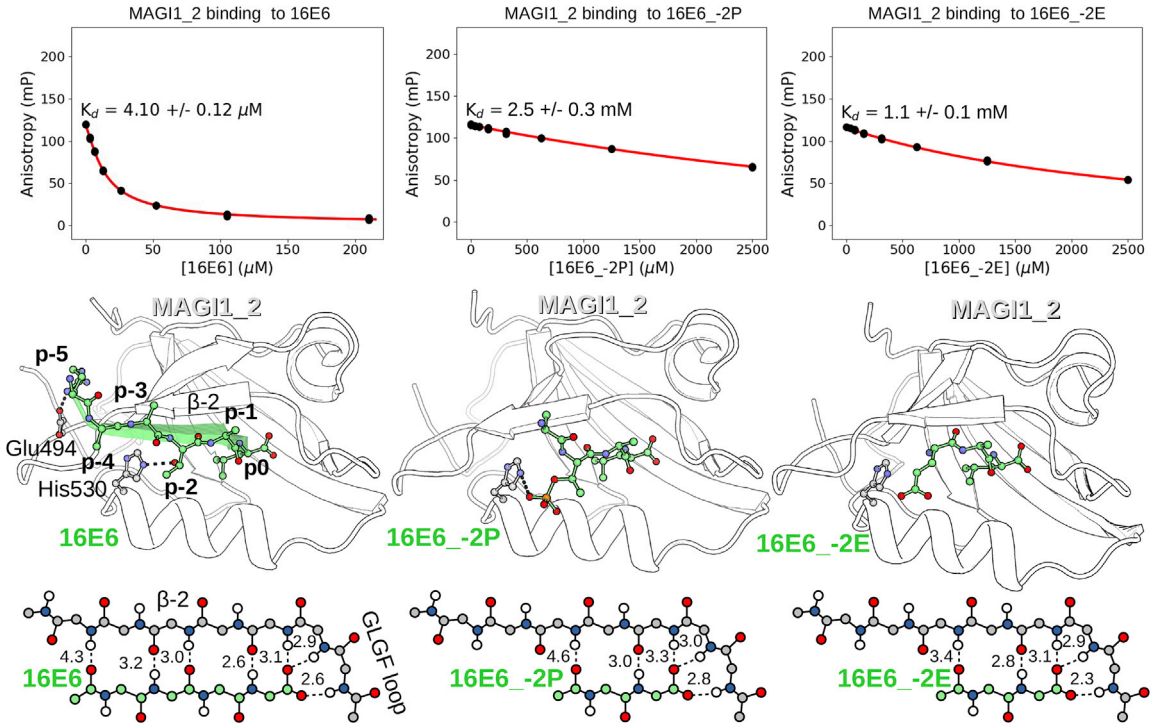

Figure 7. Crystal Structures Show the Molecular Consequence of 16E6 Phosphorylation on MAGI1_2 PDZ Binding

Isomorphous MAGI1_2-bound 16E6 peptides are shown in parallel with their affinities. Competitive fluorescence polarization assay was used to monitor the binding of 16E6 peptides to this PDZ domain (see Figure S1 for further details). 16E6 is modified at its position -2, which is involved in a bond with His530 in most class 1 PBZ/PBM complexes. Upon phosphorylation, this interaction is eliminated and only a minor contact remains possible between the His residue and the phosphate group. In the weak complexes of these modified peptides, the secondary structure of the peptide is also disturbed and the peptide seems to not adopt an optimized β strand conformation. The lower panels show the main-chain-mediated contacts (distances are given between non-hydrogen atoms). See Table S3 for statistical details of crystallographic data collection and refinement.

PBM, indicating that phosphorylation at key position -2 still allowed a residual binding mode compatible with our crystal structure of the MAGI1_2 bound 16E6_-2P peptide.

Out of all the putative PBM phosphorylation sites analyzed in this study, we have found that 1,507 PBMs are also putative binders of the 14-3-3 family, thereby presenting characteristics of dual specificity motifs (Van Roey et al., 2012). In these interactomic rearrangements, phosphorylation has a strong impact. Although some 14-3-3 binding affinities may seem moderate (like that of the 16E6/14-3-3σ interaction documented here), they may be relevant *in cellulo* since 14-3-3 isoforms are present at a high concentration in many tissues (Boston et al., 1982). Thus, an extensive dynamic interplay is likely to occur between the PDZ and 14-3-3 interaction networks. Moreover, phosphorylatable PBMs that are capable of binding PDZ and 14-3-3 proteins are also expected to bind transiently to kinases and phosphatases. That a motif bears information for the recognition by at least four different protein families has particular evolutionary consequences, since each interaction mode should impose its own constraints. This is remarkably illustrated by the HPV16 E6 PBM, which we captured here in crystal structures of two different types of complexes, one with a PDZ family member and one with a 14-3-3 family member. In both types of complexes, the same conserved residue of E6, namely Arg at position -5 of the PBM, was found to establish critical interactions, yet of a different nature. Furthermore, the same E6 PBM was, in our hands, very efficiently phosphorylated by protein kinase A (Figure S3). This kinase, as well as other members of the kinome, preferably acts on target consensus sequence presenting an Arg residue three positions upstream of the target threonine residue, i.e., precisely at the position of Arg-5 (Sarabia-Vega and Banks, 2019). The PBM of HPV16 E6 viral oncoprotein thus appears to have evolved sequence features that place it at a crossroad of four important protein families participating in the intricate, dynamic PPI network of the host organism.

PBM phosphorylation may affect not only the bound conformation, but also the free form of the motif. In the case of RSK1, we already showed that the free phosphorylated peptide adopts a transient structure in solution, where the phosphate group is involved in interactions with its preceding basic residues (Gógl et al., 2018). This intra-molecular interaction not only masks the strong negative charge of the phospho-residue, but also masks the site against inter-molecular interaction partners as it introduces an extra conformational selection step in the binding process. Such effects modulate both the kinetics and thermodynamics of the interaction. In the case of a phosphomimetic substitution, such transient charge-clamp interaction might not be as stable, resulting in a more accessible pseudo-phosphorylated PBM.

When Are Phosphomimetics a Lesser Evil Strategy?

Here, we presented a comprehensive quantitative interactomic approach to study the global effect of a PTM and its mimetic mutant

A

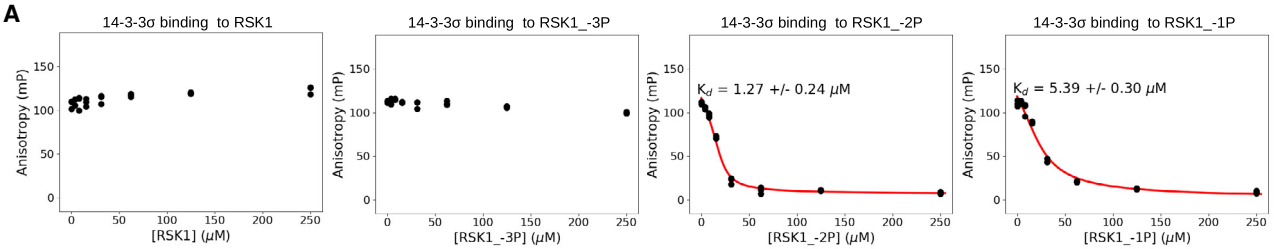

B

position	-3	-2	-1	0	$
class 1	x	[ST]	x	[LVI]	$
class 2	x	[VYF]	x	[LVI]	$
class 3	x	[ED]	x	[LVI]	$
mode III^0	x	x	[ST][^P]		$
mode III^1	x	[ST][^P]	x		$
mode III^2	[ST][^P]	x	x		$

C

	Phosphorylatable class 1 PBM		Phosphorylatable class 2 PBM	Phosphorylatable class 3 PBM
Position	No. motifs (PhosphoSite)	Putative mode III 14-3-3 binder	Putative mode III 14-3-3 binder	Putative mode III 14-3-3 binder
-1	172 (43)	172 (43)	73 (13)	59 (15)
-2	956 (113)	922 (108)	*not possible*	*not possible*
-3	138 (12)	138 (12)	80(13)	63 (9)
-4	134 (18)	*not possible*	*not possible*	*not possible*

Figure 8. Phosphorylated PBMs Are Potential 14-3-3 Binding Partners

(A) The phosphorylation of RSK1 PBM (… RKLPSTTL-COOH), affecting positions -1, -2, and -3, creates a putative mode III 14-3-3 binding site. Competitive fluorescence polarization assay was used to monitor the binding of RSK1 peptides to this 14-3-3 isoform (see Figure S4 for further details). Phosphorylation of these sites indeed increases RSK1 binding affinity to the 14-3-3σ isoform.

(B) The consensus of mode III 14-3-3 binding motifs and PBMs share some similarities. Mode III motifs require the phosphate group at positions -1, -2, or -3 and does not allow a Pro residue immediately after the phospho-residue. Positions are numbered based on the PBM numbering scheme. Numbers in the superscript indicates the linker between the phospho-residue and the C-terminal residue.

(C) According to the limitation presented in (B), most of the phosphorylatable PBMs (modified at positions -1, -2, or -3) fit into the consensus of mode III 14-3-3 binding motifs and only some class 1 motifs, phosphorylated at their -2 position, are excluded as a potential 14-3-3 binder. Numbers in parentheses indicate the number of motifs that were found to be phosphorylated in low- or high-throughput mass spectrometry datasets. $ denotes the C terminus (-COOH).

alternative on the PDZome-binding profiles of two PBMs. We further refined our previously described approach, which consists in experimentally measuring the affinities of all the possible interactions within the studied PPI network. This approach allows not only to demonstrate that phosphorylation can alter some particular interactions but also to exhaustively analyze, in quantitative terms, phosphorylation-dependent dynamics of the PDZ-PBM interactome. We hope that such approaches, which address domain-motif affinities and specificities and their potential PTM-induced changes for all possible interactions, rather than for a few selected ones, will be progressively adopted by the research community.

In an *in vitro* experiment, the phosphomimetic approach can be avoided by using a synthetic phospho-peptide, by phosphorylating a purified protein with a kinase, or by directly incorporating phospho residues during translation (Rogerson et al., 2015; Zhu et al., 2019). This is more difficult to achieve in a cellular assay. One can either activate specific pathways with external stimuli or treat the cells with phosphatase inhibitors to exceed basal phosphorylation levels of the target. However neither of these strategies will result in a pure, homogeneous phospho-state. Moreover the effect will not be specific for a single PTM site, since a huge number of phosphorylation or dephosphorylation events may simultaneously hit other sites within the same protein and in other ones. Because of its ease of use, the introduction of acidic residues to replace phosphorylated Ser/Thr residues will probably remain common in cellular (and even in *in vitro*) assays (Caria et al., 2019; Baliova and Jursky, 2019; Sundell et al., 2018).

Our study should raise further awareness about how the chemical discrepancy between phosphorylation and phosphomimetic substitution is prone to lead to quantitative binding discrepancies on an interactomic scale. Although a phosphomimetic substitution might be sufficient to reproduce the effect of a steric, structural clash induced by phosphorylation, it is likely to fail to imitate phosphorylation events that introduce novel interactions or even just modulate them, as exemplified here with 16E6 and RSK1, respectively. This limitation of the phosphomimetic strategy has already been stressed in other studies (Toto et al., 2017; Sundell et al., 2018). In addition, one should keep in mind that each motif can have multiple interaction partners (such as various PDZ domains and 14-3-3 proteins in the case of a PBM), due to their promiscuous binding properties. Although a phosphomimetic mutation may sometimes reproduce the effect of a phosphorylation for one particular interaction, it will fail to do so for many others. After all, a carboxyl group is not chemically identical to a phosphate ester.

STAR★METHODS

Detailed methods are provided in the online version of this paper and include the following:

- KEY RESOURCES TABLE
- LEAD CONTACT AND MATERIALS AVAILABILITY
- EXPERIMENTAL MODEL AND SUBJECT DETAILS
- METHOD DETAILS
  - 1. MBP-PDZ Library Preparation, Peptide Synthesis
  - 2. Holdup Assay

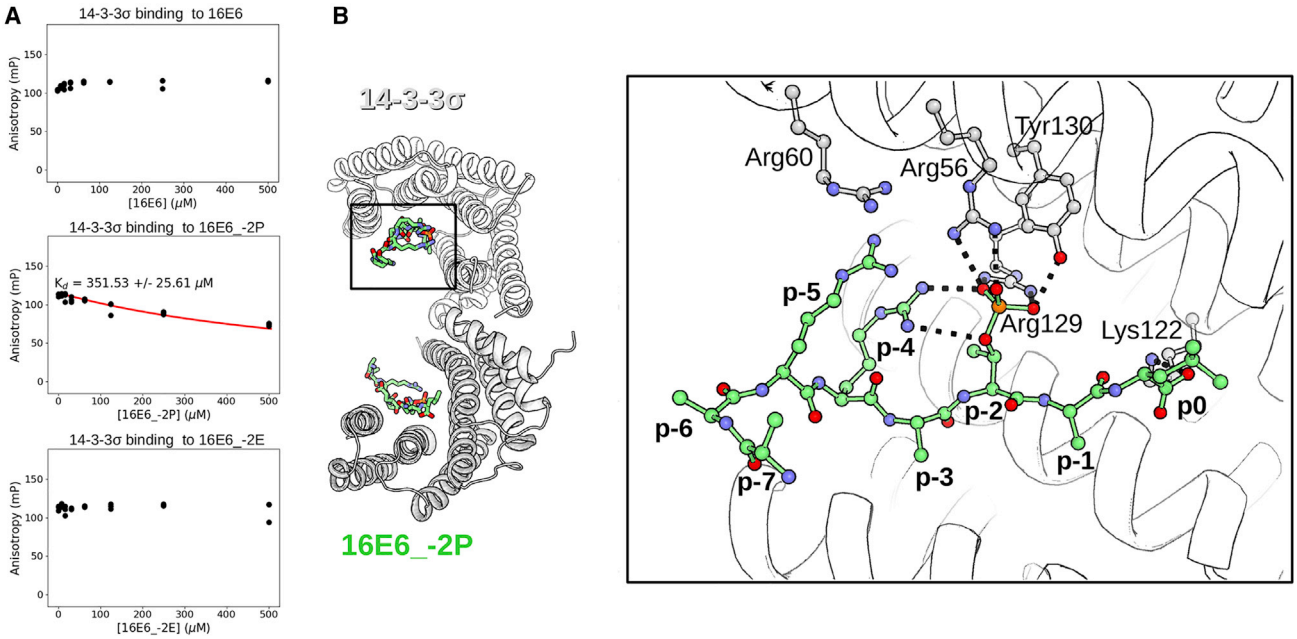

Figure 9. The Crystal Structure between 14-3-3σ and 16E6_-2P Shows the Molecular Details of a Phosphorylated PBM Bound to a 14-3-3 Protein

(A) Competitive fluorescence polarization assay was used to monitor the binding of 16E6 peptides to this 14-3-3 isoform (see Figure S4 for further details). 16E6 PBM can interact with 14-3-3σ in a phosphorylation-dependent manner.

(B) Crystal structure of 14-3-3σ bound to phosphorylated 16E6. 14-3-3 proteins form homodimers that capture two identical phosphopeptides. The inset shows the molecular determinants of the interaction. The phosphorylated residue is tightly coordinated and the C terminus of the peptide interacts with Lys122 of 14-3-3σ.

SUPPLEMENTAL INFORMATION

Supplemental Information can be found online at https://doi.org/10.1016/j.str.2020.03.010.

ACKNOWLEDGMENTS

We thank Lawrence Banks for the shared plasmids and the useful discussions. We give thanks for the support of the Swiss Light Source synchrotron (P. Scherrer Institute, Villigen, Switzerland) and the help of the beam-scientist at the PXIII beamline. The work was also supported by the Ligue Contre le Cancer (Équipe Labellisée 2015 to G.T.), the French Infrastructure for Integrated Structural Biology (FRISBI), Instruct-ERIC, and by the European Union (PDZnet network, Marie Sklodowska-Curie grant no. 675341 to G.T. and P.J.). G.G. was supported by the Post-doctorants en France program of the Fondation ARC. N.N.S. is grateful to Kristina V. Tugaeva for help with sample preparation, purification and characterization and for general discussions, as well as to the Russian Science Foundation for the grant no. 19-74-10031.

AUTHOR CONTRIBUTIONS

G.G. carried out the fluorescence polarization experiments, performed the crystallographic studies, analyzed the data, and wrote the paper. P.J. analyzed the data and performed bioinformatic analysis. P.J., C.C.-S., C.K., G.B., and N.W. performed and analyzed the holdup experiments. A.C.-S. and N.N.S. contributed to the crystallographic experiments. Y.N., L.N., R.V., and N.N.S. contributed to data analysis and data interpretation. G.T. supervised the research, analyzed the data and wrote the paper.

DECLARATION OF INTERESTS

The authors declare no conflict of interest.

Received: February 4, 2020
Revised: March 12, 2020
Accepted: March 20, 2020
Published: April 14, 2020

REFERENCES

Adams, P.D., Afonine, P.V., Bunkóczi, G., Chen, V.B., Davis, I.W., Echols, N., Headd, J.J., Hung, L.-W., Kapral, G.J., Grosse-Kunstleve, R.W., et al. (2010). PHENIX: a comprehensive Python-based system for macromolecular structure solution. Acta Crystallogr. D Biol. Crystallogr. *66*, 213–221.

Baliova, M., and Jursky, F. (2019). Phosphomimetic mutation of glycine transporter GlyT1 C-terminal PDZ binding motif inhibits its interactions with PSD95. J. Mol. Neurosci. *70*, 488–493.

Banks, L., Pim, D., and Thomas, M. (2012). Human tumour viruses and the deregulation of cell polarity in cancer. Nat. Rev. Cancer *12*, 877–886.

Boisguerin, P., Ay, B., Radziwill, G., Fritz, R.D., Moelling, K., and Volkmer, R. (2007). Characterization of a putative phosphorylation switch: adaptation of SPOT synthesis to analyze PDZ domain regulation mechanisms. ChemBioChem *8*, 2302–2307.

Boon, S.S., and Banks, L. (2013). High-risk human papillomavirus E6 oncoproteins interact with 14-3-3ζ in a PDZ binding motif-dependent manner. J. Virol. *87*, 1586–1595.

Boon, S.S., Tomaić, V., Thomas, M., Roberts, S., and Banks, L. (2015). Cancer-causing human papillomavirus E6 proteins display major differences in the phospho-regulation of their PDZ interactions. J. Virol. *89*, 1579–1586.

Boston, P.F., Jackson, P., and Thompson, R.J. (1982). Human 14-3-3 protein: radioimmunoassay, tissue distribution, and cerebrospinal fluid levels in patients with neurological disorders. J. Neurochem. *38*, 1475–1482.

Caria, S., Stewart, B.Z., Jin, R., Smith, B.J., Humbert, P.O., and Kvansakul, M. (2019). Structural analysis of phosphorylation-associated interactions of human MCC with Scribble PDZ domains. FEBS J. *286*, 1–16.

Cavet, M.E., Lehoux, S., and Berk, B.C. (2003). 14-3-3β is a p90 ribosomal S6 kinase (RSK) isoform 1-binding protein that negatively regulates RSK kinase activity. J. Biol. Chem. *278*, 18376–18383.

Charbonnier, S., Nominé, Y., Ramírez, J., Luck, K., Chapelle, A., Stote, R.H., Travé, G., Kieffer, B., and Atkinson, R.A. (2011). The structural and dynamic response of MAGI-1 PDZ1 with noncanonical domain boundaries to the binding of human papillomavirus E6. J. Mol. Biol. *406*, 745–763.

Clairfeuille, T., Mas, C., M Chan, A.S., Yang, Z., Tello-Lafoz, M., Chandra, M., Widagdo, J., Kerr, M.C., Paul, B., Teasdale, R.D., et al. (2016). A molecular code for endosomal recycling of phosphorylated cargos by the SNX27-retromer complex. Nat. Struct. Mol. Biol. *23*, 921–932.

Coblitz, B., Wu, M., Shikano, S., and Li, M. (2006). C-terminal binding: an expanded repertoire and function of 14-3-3 proteins. FEBS Lett. *580*, 1531–1535.

Cohen, N.A., Brenman, J.E., Snyder, S.H., and Bredt, D.S. (1996). Binding of the inward rectifier K+ channel Kir 2.3 to PSD-95 is regulated by protein kinase A phosphorylation. Neuron *17*, 759–767.

Davey, N.E., Van Roey, K., Weatheritt, R.J., Toedt, G., Uyar, B., Altenberg, B., Budd, A., Diella, F., Dinkel, H., and Gibson, T.J. (2012). Attributes of short linear motifs. Mol. Biosyst. *8*, 268–281.

Duhoo, Y., Girault, V., Turchetto, J., Ramond, L., Durbesson, F., Fourquet, P., Nominé, Y., Cardoso, V., Sequeira, A.F., Brás, J.L.A., et al. (2019). High throughput production of a newly designed library of soluble human single and tandem PDZ domains allows semi-quantitative PDZ-peptide interaction screening through high throughput holdup assay. Methods Mol. Biol. *2025*, 439–476.

Ecsédi, P., Gógl, G., Hóf, H., Kiss, B., Harmat, V., and Nyitray, L. (2020). Structure determination of the transactivation domain of p53 in complex with S100A4 using annexin A2 as a crystallization chaperone. Sneak Peek. https://doi.org/10.2139/ssrn.3509911.

Espejo, A.B., Gao, G., Black, K., Gayatri, S., Veland, N., Kim, J., Chen, T., Sudol, M., Walker, C., and Bedford, M.T. (2017). PRMT5 C-terminal phosphorylation modulates a 14-3-3/PDZ interaction switch. J. Biol. Chem. *292*, 2255–2265.

Ganti, K., Massimi, P., Manzo-merino, J., Tomai, V., Pim, D., and Banks, L. (2016). Interaction of the human papillomavirus E6 oncoprotein with sorting nexin 27 modulates endocytic cargo transport pathways. PLoS Pathog *12*, 1–22.

Gógl, G., Biri-Kovács, B., Póti, Á.L., Vadászi, H., Szeder, B., Bodor, A., Schlosser, G., Ács, A., Turiák, L., Buday, L., et al. (2018). Dynamic control of RSK complexes by phosphoswitch-based regulation. FEBS J. *285*, 46–71.

Gógl, G., Biri-Kovács, B., Durbesson, F., Jane, P., Nomine, Y., Kostmann, C., Bilics, V., Simon, M., Reményi, A., Vincentelli, R., et al. (2019). Rewiring of RSK-PDZ interactome by linear motif phosphorylation. J. Mol. Biol. *431*, 1234–1249.

Hornbeck, P.V., Zhang, B., Murray, B., Kornhauser, J.M., Latham, V., and Skrzypek, E. (2015). PhosphoSitePlus, 2014: mutations, PTMs and recalibrations. Nucleic Acids Res. *43*, D512–D520.

Hung, A.Y., and Sheng, M. (2002). PDZ domains: structural modules for protein complex assembly. J. Biol. Chem. *277*, 5699–5702.

Hunter, T. (2012). Why nature chose phosphate to modify proteins. Philos. Trans. R. Soc. B Biol. Sci. *367*, 2513–2516.

Ivarsson, Y., and Jemth, P. (2019). Affinity and specificity of motif-based protein-protein interactions. Curr. Opin. Struct. Biol. *54*, 26–33.

James, C.D., and Roberts, S. (2016). Viral interactions with PDZ domain-containing proteins—an oncogenic trait? Pathogens *5*, 1–22.

Javier, R.T., and Rice, A.P. (2011). Emerging theme: cellular PDZ proteins as common targets of pathogenic viruses. J. Virol. *85*, 11544–11556.

Kabsch, W. (2010). Xds. Acta Crystallogr. D Biol. Crystallogr. *66*, 125–132.

Krystkowiak, I., and Davey, N.E. (2017). SLiMSearch: a framework for proteome-wide discovery and annotation of functional modules in intrinsically disordered regions. Nucleic Acids Res. *45*, W464–W469.

Kühne, C., Gardiol, D., Guarnaccia, C., Amenitsch, H., and Banks, L. (2000). Differential regulation of human papillomavirus E6 by protein kinase A: conditional degradation of human discs large protein by oncogenic E6. Oncogene *19*, 5884–5891.

Kumar, M., Gouw, M., Michael, S., Sámano-Sánchez, H., Pancsa, R., Glavina, J., Diakogianni, A., Valverde, J.A., Bukirova, D., Čalyševa, J., et al. (2019). ELM—the eukaryotic linear motif resource in 2020. Nucleic Acids Res. *48*, 1–11.

Luck, K., Fournane, S., Kieffer, B., Masson, M., Nominé, Y., and Travé, G. (2011). Putting into practice domain-linear motif interaction predictions for exploration of protein networks. PLoS One *6*, e25376.

Luck, K., Charbonnier, S., and Travé, G. (2012). The emerging contribution of sequence context to the specificity of protein interactions mediated by PDZ domains. FEBS Lett. *586*, 2648–2661.

Lucrèce, M., Emmanuelle, S., Fabienne, B., Sandrine, S., Olivier, L., and Gérard, B. (2011). Sequence-dependent enrichment of a model phosphopeptide: a combined MALDI-TOF and NMR study. Anal. Chem. *83*, 3003–3010.

McCoy, A.J., Grosse-Kunstleve, R.W., Adams, P.D., Winn, M.D., Storoni, L.C., and Read, R.J. (2007). Phaser crystallographic software. J. Appl. Crystallogr. *40*, 658–674.

Narayana, N., Cox, S., Shaltiel, S., Taylor, S.S., and Xuong, N.H. (1997). Crystal structure of a polyhistidine-tagged recombinant catalytic subunit of cAMP-dependent protein kinase complexed with the peptide inhibitor PKI(5-24) and adenosine. Biochemistry *36*, 4438–4448.

Obsil, T., and Obsilova, V. (2011). Structural basis of 14-3-3 protein functions. Semin. Cell Dev. Biol. *22*, 663–672.

Panni, S., Montecchi-Palazzi, L., Kiemer, L., Cabibbo, A., Paoluzi, S., Santonico, E., Landgraf, C., Volkmer-Engert, R., Bachi, A., Castagnoli, L., et al. (2011). Combining peptide recognition specificity and context information for the prediction of the 14-3-3-mediated interactome in *S. cerevisiae* and *H. sapiens*. Proteomics *11*, 128–143.

Pearlman, S.M., Serber, Z., and Jr, J.E.F. (2011). A mechanism for the evolution of phosphorylation sites. Cell *147*, 934–946.

Roehrl, M.H.A., Wang, J.Y., and Wagner, G. (2004). A general framework for development and data analysis of competitive high-throughput screens for small-molecule inhibitors of protein-protein interactions by fluorescence polarization. Biochemistry *43*, 16056–16066.

Van Roey, K., Gibson, T.J., and Davey, N.E. (2012). Motif switches: decision-making in cell regulation. Curr. Opin. Struct. Biol. *22*, 378–385.

Rogerson, D.T., Sachdeva, A., Wang, K., Haq, T., Kazlauskaite, A., Hancock, S.M., Huguenin-Dezot, N., Muqit, M.M.K., Fry, A.M., Bayliss, R., et al. (2015). Efficient genetic encoding of phosphoserine and its nonhydrolyzable analog. Nat. Chem. Biol. *11*, 496–503.

Sarabia-Vega, V., and Banks, L. (2019). Acquisition of a phospho-acceptor site enhances HPV E6 PDZ-binding motif functional promiscuity. J. Gen. Virol. https://doi.org/10.1099/jgv.0.001236.

Shi, G.-X., Yang, W.S., Jin, L., Matter, M.L., and Ramos, J.W. (2018). RSK2 drives cell motility by serine phosphorylation of LARG and activation of Rho GTPases. Proc. Natl. Acad. Sci. U S A *115*, E190–E199.

Sieracki, N.A., and Komarova, Y.A. (2013). Studying cell signal transduction with biomimetic point mutations. In Genetic Manipulation of DNA and Protein - Examples from Current Research, D. Figurski, ,, ed. (IntechOpen).

Simon, M., Gógl, G., Ecsédi, P., Póti, Á., Kardos, J., and Nyitray, L. (2020). High throughput competitive fluorescence polarization assay reveals functional redundancy in the S100 protein family. FEBS J. 1–13.

Sluchanko, N.N. (2018). Association of multiple phosphorylated proteins with the 14-3-3 regulatory hubs: problems and perspectives. J. Mol. Biol. *430*, 20–26.

Sluchanko, N.N., Beelen, S., Kulikova, A.A., Weeks, S.D., Antson, A.A., Gusev, N.B., and Strelkov, S.V. (2017). Structural basis for the interaction of a human small heat shock protein with the 14-3-3 universal signaling regulator. Structure *25*, 305–316.

Songyang, Z., Fanning, A.S., Fu, C., Xu, J., Marfatia, S.M., Chishti, A.H., Crompton, A., Chan, A.C., Andersen, J.M., and Cantley, L.C. (1997). Recognition of unique carboxyl-terminal motifs by distinct PDZ domains. Science *275*, 73–77.

Suarez, I., and Trave, G. (2018). Structural insights in multifunctional papillomavirus oncoproteins. Viruses *10*, 1–22.

Sundell, G.N., Arnold, R., Ali, M., Naksukpaiboon, P., Orts, J., Güntert, P., Chi, C.N., and Ivarsson, Y. (2018). Proteome-wide analysis of phospho-regulated PDZ domain interactions. Mol. Syst. Biol. *14*, 1–22.

Thomas, G.M., Rumbaugh, G.R., Harrar, D.B., and Huganir, R.L. (2005). Ribosomal S6 kinase 2 interacts with and phosphorylates PDZ domain-containing proteins and regulates AMPA receptor transmission. Proc. Natl. Acad. Sci. U S A *102*, 15006–15011.

Thomas, M., Myers, M.P., Massimi, P., Guarnaccia, C., and Banks, L. (2016). Analysis of multiple HPV E6 PDZ interactions defines type-specific PDZ fingerprints that predict oncogenic potential. Plos Pathog. *12*, 1–21.

Toto, A., Mattei, A., Jemth, P., Gianni, S., Biochimiche, S., Fanelli, A.R., Pasteur, I., Cenci, F., Molecolari, P., Università, S., et al. (2017). Understanding the role of phosphorylation in the binding mechanism of a PDZ domain. Protein Eng. *30*, 1–5.

Vaccaro, P., and Dente, L. (2002). PDZ domains: troubles in classification. FEBS Lett. *512*, 345–346.

Vincentelli, R., Luck, K., Poirson, J., Polanowska, J., Abdat, J., Blémont, M., Turchetto, J., Iv, F., Ricquier, K., Straub, M.-L., et al. (2015). Quantifying domain-ligand affinities and specificities by high-throughput holdup assay. Nat. Methods *12*, 787–793.

Zhang, Y., Dasgupta, J., Ma, R.Z., Banks, L., Thomas, M., and Chen, X.S. (2007). Structures of a human papillomavirus (HPV) E6 polypeptide bound to MAGUK proteins: mechanisms of targeting tumor suppressors by a high-risk HPV oncoprotein. J. Virol. *81*, 3618–3626.

Zheng, W., Zhang, Z., Ganguly, S., Weller, J.L., Klein, D.C., and Cole, P.A. (2003). Cellular stabilization of the melatonin rhythm enzyme induced by nonhydrolyzable phosphonate incorporation. Nat. Struct. Biol. *10*, 1054–1057.

Zhu, P., Gafken, P.R., Mehl, R.A., and Cooley, R.B. (2019). A highly versatile expression system for the production of multiply phosphorylated proteins. ACS Chem. Biol. *14*, 1564–1572.

STAR★METHODS

KEY RESOURCES TABLE

REAGENT or RESOURCE	SOURCE	IDENTIFIER
Bacterial and Virus Strains		
Bacteria: E.coli BL21(DE3)	NEB	Cat#C2527I
Chemicals, Peptides, and Recombinant Proteins		
RSK1 peptide	(Gógl et al., 2019)	N/A
RSK1_-1P peptide	This paper	N/A
RSK1_-2P peptide	This paper	N/A
RSK1_-3P peptide	(Gógl et al., 2019)	N/A
RSK1_-3E peptide	This paper	N/A
16E6 peptide	(Vincentelli et al., 2015)	N/A
16E6_-2P peptide	This paper	N/A
16E6_-2E peptide	This paper	N/A
pB6 peptide	Severn Biotech	N/A
Deposited Data		
Crystal structure of RSK1 + MAGI1_2	(Gógl et al., 2018)	PDB ID: 5N7D
Crystal structure of RSK1_-3P + MAGI1_2	(Gógl et al., 2018)	PDB ID: 5N7F
Crystal structure of RSK1_-3E + MAGI1_2	This paper	PDB ID: 6TWY
Crystal structure of 16E6 + MAGI1_2	This paper	PDB ID: 6TWQ
Crystal structure of 16E6_-2P + MAGI1_2	This paper	PDB ID: 6TWX
Crystal structure of 16E6_-2E + MAGI1_2	This paper	PDB ID: 6TWU
Crystal structure of 16E6_-2P + 14-3-3σ	This paper	PDB ID: 6TWZ
Recombinant DNA		
PDZome library (His6-MBP-PDZ constructs in modified pET15b)	(Duhoo et al., 2019)	N/A
Plasmid: ANXA2-fused MAGI1_2 (His6-tagged in modified pET15b)	(Gógl et al., 2018)	N/A
Plasmid: 14-3-3σ (His6-tagged in modified pET28)	(Sluchanko et al., 2017)	N/A
Plasmid: 14-3-3σ optimized for crystallization (His6-tagged in modified pET28)	(Sluchanko et al., 2017)	N/A
Plasmid: PKA (His6-tagged in pET15b)	Narayana et al., 1997	Addgene Plasmid #14921
Software and Algorithms		
XDS	(Kabsch, 2010)	xds.mpimf-heidelberg.mpg.de/
Phaser	(McCoy et al., 2007)	www.phenix-online.org
Phenix	(Adams et al., 2010)	www.phenix-online.org
ProFit	(Simon et al., 2020)	github.com/GoglG/ProFit

LEAD CONTACT AND MATERIALS AVAILABILITY

Further information and requests for resources and reagents should be directed to and will be fulfilled by the Lead Contact, Gergo Gogl (goglg@igbmc.fr). The study did not generate new unique reagents.

EXPERIMENTAL MODEL AND SUBJECT DETAILS

The study focused on human proteins and peptides, expressed in E. coli BL21(DE3) or synthesized chemically.

METHOD DETAILS

1. MBP-PDZ Library Preparation, Peptide Synthesis

We used an updated version of our original PDZome library, that contains all the human (266) PDZ domains as soluble, isolated His6-MBP-PDZ constructs. This PDZome v2 library was prepared as previously described in details (Duhoo et al., 2019). Briefly, His6-MBP-PDZ constructs were individually overexpressed in E. coli BL21(DE3) with an autoinduction media. The His6-MBP-PDZ concentrations of soluble cell lysate fractions were evaluated with a microfluidic capillary electrophoretic system (Caliper LabChip GXII, PerkinElmer, Waltham, Massachusetts) and were adjusted to 4 μM by dilutions.

Tandem affinity purified proteins were used for affinity measurements. His6-MBP-PDZ constructs were purified on a Ni-IDA column and they was further purified by amylose affinity chromatography. For crystallization, ANXA2-fused MAGI1_2 was captured on a Ni-IDA column, the His6 tag was removed with a TEV protease and the protein was purified by cation exchange on a HiTrap SP HP column (GE Healthcare, Chicago, Illinois).

For affinity measurements an N-terminally His6-tagged 14-3-3σ (1-231) protein was used that lacked its flexible C-terminal extension. For crystallization, an engineered version of this protein was used, carrying amino acid substitutions 159KKE161 -> 159AAA161 to reduce surface entropy (Sluchanko et al., 2017). Both 14-3-3 proteins were expressed in E. coli BL21(DE3) and purified by Ni-affinity chromatography and gel-filtration. In the case of the engineered isoform, the expression tag was removed with 3C protease followed by a reverse Ni-affinity purification and gel-filtration.

Peptides used for holdup experiments (16E6: biotin-ttds-SSRTRRETQL; 16E6_-2P: biotin-ttds-SSRTRREpTQL; 16E6_-2E: biotin-ttds-SSRTRREEQL; RSK1: biotin-ttds-RRVRKLPSTTL; RSK1_-3P: biotin-ttds-RRVRKLPpSTTL; RSK1_-3E: biotin-ttds-RRVRKLPETTL) and the fluorescent peptides (f16E6: fluorescein-RTRRETQL; fRSK1: fluorescein-KLPSTTL and fpRSK1: fluorescein-KLPpSTTL) were chemically synthesized on an ABI 443A synthesizer with Fmoc strategy. In all cases, the biotin group was attached to the N-terminus via a TTDS linker and fluorescein was coupled directly to the N-terminus. The pB6 peptide (WLRRApSAPLPGLK) was commercially purchased (Severn Biotech, Kidderminster, UK). Predicted peptide masses were confirmed by mass-spectrometry.

His6-tagged PKA (Addgene #14921) (Narayana et al., 1997) was expressed in E. coli BL21(DE3) and was purified on a Ni-IDA column. Kinase reaction on f16E6 (800 μM) was performed in the presence of 5 mM MgCl2 and 2 mM ATP and 50 μM kinase for 3 h at room temperature. The kinase was removed from the reaction by boiling and centrifugation and the remaining peptide solution was buffer exchanged. pB6 peptide was labeled with sub-stoichiometric FITC (Sigma-Aldrich, St. Louis, Missouri) in a basic HEPES buffer (pH 8.2) and the reaction was stopped with 100 mM TRIS. The peptide was buffer exchanged in order to separate from the fluorescent contaminants.

The concentration of proteins, or peptides that contained aromatic residues were determined by their UV absorption at 280 nm. The concentration of peptide solutions which lacked aromatic residues were estimated based on the dry mass of the peptides and later confirmed by their far UV absorption (at 205 and 214 nm).

2. Holdup Assay

The automated holdup assay was carried out with the peptides 16E6, 16E6_-2P, 16E6_-2E, RSK1_-3P and RSK1_-3E in singlicates using a previously described protocol. (As 16E6 was used as a benchmark peptide for the new PDZome library, we measured its binding profile at least 5 times.) First, streptavidin resin was saturated with biotinylated peptides or with biotin (as a negative control). Then, the resins were depleted with an excess of biotin and were washed with a biotin-free buffer. Concentration-adjusted His6-MBP-PDZ containing cell lysates (PDZome v2 library) were incubated with the resins for a sufficient time for complex formation (30 min). The supernatant was separated from the resin by a fast filtration step, carried out by using filter plates (Millipore, Burlington, Massachusetts). PDZ concentrations were evaluated using a microcapillary electrophoretic system (Caliper; PerkinElmer, Waltham, Massachusetts) and BI values were calculated using Equation 1.

$$BI = \frac{I_{total} - I_{depleted}}{I_{total}} \quad \text{(Equation 1)}$$

where Itotal is the total Intensity of the PDZ peak (measured by the biotin control) and Idepleted is the intensity of PDZ peak in the peptide depleted reaction. In the holdup buffer at least a single internal standard was used (BSA and/or lysozyme) for peak intensity normalization (Figure S2).

3. Fluorescence Polarization (FP) Assay

Fluorescence polarization was measured with a PHERAstar (BMG Labtech, Offenburg, Germany) microplate reader by using 485 ± 20 nm and 528 ± 20 nm band-pass filters (for excitation and emission, respectively). In direct FP measurements, a dilution series of the MBP-PDZ or 14-3-3 protein was prepared in 96 well plates (96 well skirted pcr plate, 4ti-0740, 4titude, Wotton, UK) in a 20 mM HEPES pH 7.5 buffer that contained 150 mM NaCl, 0.5 mM TCEP, 0,01% Tween 20 and 50 nM fluorescently-labeled peptide. The volume of the dilution series was 40 μl, which was later divided into three technical replicates of 10 μl during transferring to 384 well micro-plates (low binding microplate, 384 well, E18063G5, Greiner Bio-One, Kremsmünster, Austria). In total, the polarization of the probe was measured at 8 different protein concentrations (whereas one contained no protein and corresponded to the free peptide). In competitive FP measurements, the same buffer was supplemented with the protein to achieve a complex formation of 60-80%,

based on the titration. Then, this mixture was used for creating a dilution series of the competitor (i.e. the studied peptides) and the measurement was carried out identically as in the direct experiment. Analysis of FP experiments were carried out using ProFit, an in-house developed, Python-based fitting program (Simon et al., 2020). The dissociation constant of the direct and competitive FP experiment was obtained by fitting the measured data with quadratic and competitive equation, respectively (Roehrl et al., 2004). Competitive titrations in the main figures are reproduced from Figures S1 or S4 (without their direct experimental pairs) unless it is defined differently in the text.

4. Crystallization

The MAGI1_2 complexes were reconstituted by mixing purified the ANXA2-fused PDZ domain (135 μM) and synthetic (biotinylated) peptides in a 1:3-1:15 stoichiometric ratio, depending on the dissociation constant of the crystallized complex. 14-3-3σ (300 μM) was supplemented with 16E6_-2P peptide in a 1:3 molar ratio. Crystallization conditions were screened using commercially available and in-house developed kits (Qiagen, Hampton Research, Emerald Biosystems) by the sitting-drop vapor-diffusion method in 96-well MRC 2-drop plates (SWISSCI, Neuheim, Switzerland), using a Mosquito robot (TTP Labtech, Cambridge, UK). After optimization, PDZ crystals grew rapidly in a drop made from 5 μl of protein solution and 5 μl of reservoir solution containing 20-25% polyethylene glycol 3000, 100 mM sodium citrate buffered at pH 5.5 and 100 mM trisodium-citrate at 20°C. The optimized condition of the 14-3-3σ crystals consisted of 20% polyethylene glycol 3350, 0.1M Bis-tris propane buffered at pH 6.5 and 0.2 M K/Na-tartarate at 4°C. All crystals were flash-cooled in a cryoprotectant solution containing 20% glycerol and stored in liquid nitrogen.

X-ray diffraction data were collected at the Synchrotron Swiss Light Source (SLS) (Switzerland) on the X06DA (PXIII) beamline and processed with the program XDS (Kabsch, 2010). The crystal structure was solved by molecular replacement with a previously determined crystal structure of the same chimera (PDB ID 5N7D), or with an apo 14-3-3σ structure (PDB ID 5LU2) using Phaser (McCoy et al., 2007) and structure refinement was carried out with PHENIX (Adams et al., 2010). TLS refinement was applied during the refinement. The crystallographic parameters and the statistics of data collection and refinement are shown in Table S3. The refined model and the structure factor amplitudes have been deposited in the PDB with the accession codes 6TWQ, 6TWU, 6TWX, 6TWY and 6TWZ.

A final electron density map, along with a simulated annealing difference omit map, is shown for all the determined crystal structures in Figure S5. A crystallographic dataset was also collected at a resolution of 2.9 Å of an APO ANXA2-fused MAGI1_2 crystal in order to calculate isomorphous difference maps on all the PDZ-bound complexes determined in this study.

QUANTIFICATION AND STATISTICAL ANALYSIS

1. Fluorescence Polarization Assay

The reported dissociation constants and errors are the average and the standard deviations of 500 independent Monte-Carlo simulations, calculated using ProFit as described in Simon et al., 2020.

2. Conversion of Holdup Binding Intensities to Dissociation Constants

Steady-state binding intensities (deduced from holdup assays) can be converted to steady-state dissociation constants using Equation 2:

$$K_d = \frac{([PDZ] - BI * [PDZ]) * ([PBM] - BI * [PDZ])}{BI * [PDZ]} \quad \text{(Equation 2)}$$

where [PDZ] is the total PDZ concentration (set to 4 μM in usual cases in our assays) and [PBM] is the total peptide concentration. This parameter is unknown that makes a direct and accurate conversion impossible.

To reveal this missing parameter for accurate conversion, we used the orthogonal affinity values from the fluorescence polarization assay. For each BI-Kd pairs, where both affinity measurements showed a detectable binding, we calculated an apparent peptide concentration based on Equation 2.

The calculated peptide concentrations showed a tailed distribution, with a few clear outliers in each cases. To estimate a global peptide concentration that is most compatible between every BI-Kd datasets, we performed an outlier rejection based on the absolute distances from the median (Figure 3A). Based on these criteria, we could calculate the average peptide concentration for each peptides using approximately 10 BI-Kd pairs. For the conversion of the modified 16E6 peptides, for which we lacked any reliable BI-Kd pairs, we used a peptide concentration of the average of the other peptides. We performed the conversion until the limit of detection of the holdup assay (BI = 0.1) in ‘ S2.

DATA AND CODE AVAILABILITY

The accession number for the crystal structure of RSK1_-3E + MAGI1_2 reported in this paper is PDB ID: 6TWY. The accession number for the crystal structure of 16E6 + MAGI1_2 reported in this paper is PDB ID: 6TWQ. The accession number for the crystal structure of 16E6_-2P + MAGI1_2 reported in this paper is PDB ID: 6TWX. The accession number for the crystal structure of 16E6_-2E + MAGI1_2 reported in this paper is PDB ID: 6TWU. The accession number for the crystal structure of 16E6_-2P + 14-3-3σ reported in this paper is PDB ID: 6TWZ. Any additional data, that is not directly available in the supplement, can be requested from the authors.